64. Conformational Analysis of Didemnins

A Multidisciplinary Approach by Means of X-Ray, NMR, Molecular-Dynamics, and Molecular-Mechanics Techniques

by **Horst Kessler**[1])* and **Martin Will**

Institut für Organische Chemie der Universität Frankfurt, Niederurseler Hang, D–6000 Frankfurt 50

and **Jochen Antel, Holger Beck,** and **George M. Sheldrick**

Institut für Anorganische Chemie der Universität Göttingen, Tammannstrasse 4, D–3400 Göttingen

(9.XII.88)

We present the application of several homo- and heteronuclear 1D- and 2D-NMR techniques to assign the ^{1}H-NMR chemical shifts of the dominant conformation of didemnin B (**2**; three different conformations in (D_6)DMSO solution in the ratio 8:1:1) and its conformational analysis, as well as the solution conformation of didemnin A (**1**). The conformations were refined by restrained molecular-dynamics calculations using the GROMOS program and by MOMO, a novel personal-computer-based interactive molecular-graphics and molecular-mechanics package, using experimental distances (*via* a H...H pseudo potential function) as restraints. The solution structures of **1** and **2** obtained by GROMOS and MOMO calculations were compared with each other and related to the recently solved crystal structure of **2**. Focusing on the main conformer, the two kinds of the distance-restrained conformational calculations for **2** yielded a 'solution structure' close to the crystal structure. Almost all of the 40 restrained H...H distances coincided (within the estimated standard deviations) with those observed in the crystal structure. One more hydrogen bond was detected in solution involving the lactoyl OH group (disordered in the crystal structure) and the dimethyltyrosine (Me_2Tyr^5) carbonyl O-atom. The macrocyclic ring system in the modeled solution structure of **1** exhibited a topology close to those of the solution and crystal structures of **2**. The main difference between **1** and **2** could be traced back to a significant change in the ψ angle of the *N*-methyl-D-leucine ($MeLeu^7$) residue. In **1**, the *N*-methyl moiety of $MeLeu^7$ points inward within the macrocyclic ring toward the Ist and Hip region. We also tested the suitability of structures obtained from NMR data as 'search fragments' in the '*Patterson* search approach' of crystal-structure analysis. It proved possible to resolve the crystal structure of **2** *a posteriori* with the *Patterson* search program PATSEE, in this way.

Introduction. – Didemnin A (**1**) and B (**2**); *Fig. 1* belong to a new class of highly active antiviral cytotoxic depsipeptides which were isolated from a Caribbean tunicate of the family Didemnidae *(Tridemnum genus)*. A first structural characterization was performed by degradative and some spectroscopic studies [1] [2]. The total synthesis of the didemnins [3] [4], the crystal structure of didemnin B (**2**) [5], and the assignment of all ^{1}H- and ^{13}C-NMR signals of didemnin A (**1**) in solution [6] have been published recently. The interesting spectrum of biological activities of the didemnins (discussed below) has prompted further research on their structural features in the solid state and in solution. A detailed knowledge of the conformations in different environments is required to understand the difference in the activity between didemnin A (**1**) and B (**2**).

These cyclic depsipeptides are of great interest because of their effective inhibition of the replication of DNA and RNA viruses *in vitro* [2]. They are reported to be highly active *in vivo* against P388 leukemia and B16 melanoma and potent inhibitors of the L1210

[1]) New address: Lehrstuhl II für Organische Chemie, Technische Universität München, Lichtenbergstr. 4, D–8046 Garching.

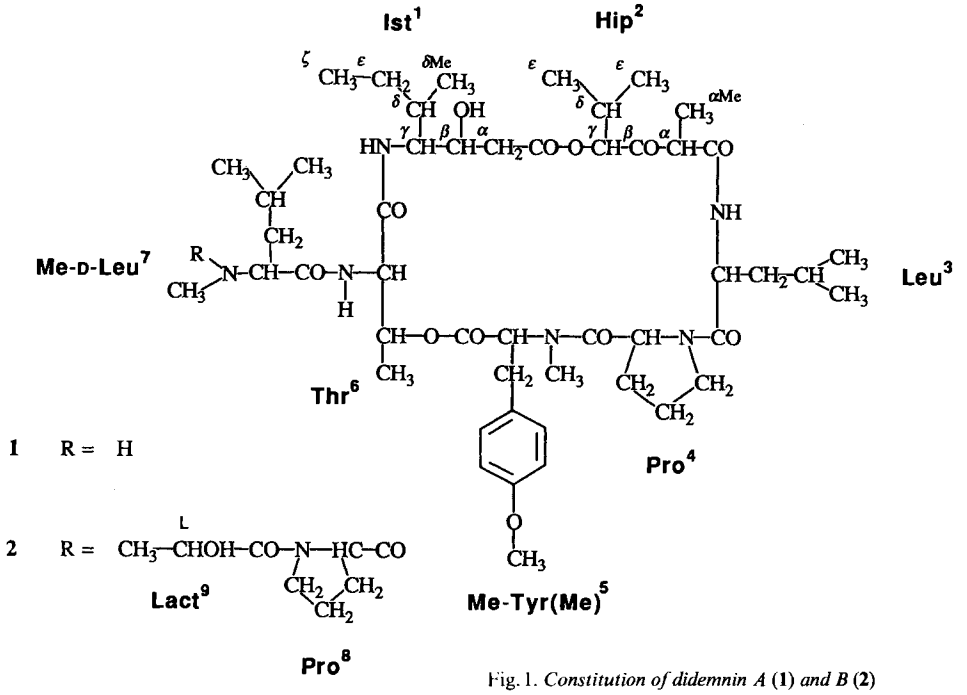

Fig. 1. *Constitution of didemnin A* (**1**) *and B* (**2**)

leukemia cells *in vitro* [3]. The didemnins show a novel cyclic depsipeptide structure containing one unit of hydroxyisovalerylpropionic acid (=(2*S*,4*S*)-4-hydroxy-2,5-dimethyl-3-oxohexanoic acid; Hip) and isostatin (=(3*S*,4*R*,5*S*)-4-amino-3-hydroxy-5-methylheptanoic acid; Ist), a new isomer of the amino acid statin. The presence of isostatine has been established by the determination of the crystal structure of didemnin (**2**) [5]. All didemnins characterized so far contain the same cyclic depsipeptide backbone, differing only by the substituent R linked to the *N*-methylleucine (MeLeu) residue. In the different biological tests [7], **2** has been 2–3 orders of magnitude more active and *ca.* 20 times more cytotoxic [8] than **1** or didemnin C. Recently, **2** is reported to show significant activity against some human tumors, such as carcinoma of the breast, ovary, kidney, and lung, mesothelioma, sarcoma, and hairy cell leukemia in the *in-vitro* tests [9] [10]. Therefore, **2** has entered clinical trials as a potential antitumor agent [11]. There have been many biological studies on the didemnins, but much less work which provides insights in the topological features of the didemnins [5]. Such information is highly required to explain the possible mechanism of the biological action of these substances and the great differences in their activities. Preliminary studies indicate that the didemnins should be protein-synthesis inhibitors but do not bind to DNA [8]. The biological behaviour of the didemnins has been compared to some other polypeptide antibiotics in order to elucidate the possible mechanism of biological interaction. Thus, it has been shown that in comparison to valinomycin or gramicidin, didemnins do not function as ionophore for sodium or potassium cations [12]. Didemnins have been compared with cyclosporine A too, because of their potent immunosupressive activity [13] and the much more potent inhibition of binding of prolactine to human lymphocytes [14]. The topological comparison [5]

reveals that the solid-state conformation of didemnin B (**2**) is more similar to the solution structure of cyclosporin A [15] than to the crystal structure of cyclosporine A. However, there are great differences in the polarity of the side chains of cyclosporine A (Me-Bmt) and **2** (*N*-lactoylproline moiety). So it seems very unlikely that the binding sites would be the same.

We report here the assignment of the ^{1}H-NMR signals of didemnin B (**2**) by the application of one- and two-dimensional NMR techniques [16]. The three-dimensional molecular structures of both didemnin A (**1**) and B (**2**) are derived from NMR data and restraint molecular dynamics (MD) and molecular-mechanics (MM) calculations.

Assignment of the NMR Signals of Didemnin B (2). – The assignment of the NMR signals is based exclusively on connectivity information *via* scalar coupling [17] [18]. We have applied various recently established NMR techniques including TOCSY experiments [19] and proton-detected heteronuclear long-range correlation experiments using semiselective C-atom pulses ('inverse COLOC') [20] for tracing out correct correlations. Three distinct sets of signals belonging to three different conformers are observed in (D_6)DMSO solution, in a relative ratio of 8:1:1. The presence of two *N*-methylated amino-acid residues in **2** and two prolines (Pro) suggest that these conformations which are slowly interconverting on the NMR time scale arise from rotational isomerism about the secondary amid bond (see below). The analysis of the three spin systems presents some pitfalls, caused by severe overlapping when examined merely by standard techniques. The digitization of the 500-MHz DQF-COSY [21] is sufficiently high to resolve three different conformations only for a part of the molecule. This part consists of the Hip, Ist, and the side-chain lactoyl (Lact) residues. The threonine (Thr) and leucine (Leu) residues exhibit only two distinct signal sets, whereas for the methyltyrosine (Me-Tyr(Me), short form: Me_2Tyr) and for each of the two Pro only one spin-system pattern can be identified. A confirmation of the resonances belonging to the less populated conformers is obtained by the inspection of exchange cross-peaks in the NOESY [16] [22] [23 a] spectra. To attain an independent proof of the occurrence of these patterns of resonances, we have recorded reference spectra of synthetically produced **2** (kindly provided by *U. Schmidt* and coworkers [4] which confirm our results). In a previous publication [6], we have described the way of assigning didemnin A (**1**) in detail; thus, we sketch out the assignment of **2** only briefly, the results being summarized in *Table 1*.

The double-quantum-filtered COSY (DQF-COSY) spectrum recorded at first yields the assignment of almost all proton signals of the main conformer. The TOCSY spectrum then allows an unambiguous assignment of all of the aliphatic side-chain protons as well and provides some redundant information to increase the reliability. Beside this, the application of the TOCSY technique leads to the assignment of the two less populated conformers (*ca.* 10% each) which will now be described concentrating on some marked features of the Ist residue. A complication is due to a missing cross-peak indicating the correlation between the low-field α and β protons owing to small coupling constant. In addition, the H–C(γ)/H–C(δ) correlation cannot be obtained. The problem is similar to the β, γ correlation in Leu residues, as pointed out for cyclosporin [17] [24]. The H–C(δ) at 1.87 ppm couples to six vicinal neighbours, yielding a broad signal of low intensity with antiphase structure of the δ, γ coupling, Hence, this cross-peak cannot be observed in the COSY spectrum. However, these missing correlations are apparent in the TOCSY, NOESY, and 'inverse COLOC' spectra [20]. For the latter technique which is based on the original pulse sequence of *L. Müller* [25], optimized for long-range coupling, a semiselective excitation of the carbonyl resonances *via Gaussian*-shaped pulses [26] is applied to provide sufficient resolution in the carbon dimension.

In the TOCSY spectrum which is recorded with the MLEV17 sequence for the spin-lock (HOHAHA) [19], the NH resonance of Ist^1, *e.g.*, exhibits correlations to the degenerate H–C(γ) and H–C(β) and to H–C(α) and

Table 1. *^{1}H-NMR Chemical Shifts* (δ [ppm]) *and Coupling Constants* ^{3}J [Hz] *of Didemnin B* (**2**) *in (D$_6$)DMSO Solution at 300 K*[a])

	Ist[1]	Hip[2]	Leu[3]	Pro[4]	Me_2Tyr[5]	Thr[6]	MeLeu[7]	Pro[8]	Lact[9]
NH	6.93 (7.20, 7.05)	–	7.85 (7.70)	–	–	7.76 (7.84)	–	–	–
^3J(NH, α or γ)	9.7	–	9.1	–	–	5.7	–	–	–
H–C(α)	3.44 (3.24, 3.40)	3.96 (3.75, 3.77)	4.63 (4.69)	4.62	4.07	4.36 (4.41)	5.22	4.70	4.36 (4.30, 4.24)
H′–C(α)	2.27 (2.18, 2.24)	–	–	–	–	–	–	–	–
CH_3–C(α)	–	1.16 (1.16, 1.15)	–	–	–	–	–	–	1.24 (1.14, 1.22)
^3J(α,β)[b])	–	–	–	8.7^S	4.6^S	2.4	11.1^S	7.8^S	–
^{3}J (α,β)[b])	–	–	–	4.5^R	11.0^R	–	5.0^R	7.4^R	–
H–C(β)	3.82 (3.79)	–	1.52 (1.55)	2.14	3.16	5.02 (4.98)	1.67	2.18	–
H′–C(β)	–	–	1.07	1.55	2.96	–	1.60	1.67	–
H–C(γ)	3.80 (3.82, 3.79)	4.90 (4.88)	1.44 (1.22)	1.97	–	1.22 (1.14)	1.36	2.05	–
H′–C(γ)	–	–	–	1.80	–	–	–	1.87	–
^3J(γ,δ)	–	3.9	–	–	–	–	–	–	–
H–C(δ)	1.87	2.24 (2.19)	0.87 (0.89)	3.60	7.15	–	0.85	3.84 (3.70)	–
H′–C(δ)	–	–	0.87 (0.89)	3.47	–	–	0.77	3.53 (3.43)	–
CH_3–C(δ)	0.83	–	–	–	–	–	–	–	–
H–C(ε)	1.24	0.83 (0.79)	–	–	6.86	–	–	–	–
H′–C(ε)	1.14	0.76 (0.74)	–	–	–	–	–	–	–
CH_3(δ)	0.86	–	–	–	–	–	–	–	–
CH_3N	–	–	–	–	2.50	–	3.06	–	–
CH_3O	–	–	–	–	3.73	–	–	–	–
OH	4.35	–	–	–	–	–	–	–	–

[a]) Values in parenthesis correspond to the minor conformers.

[b]) Superscripts *S* and *R* are used to indicate *(pro-S)* and *(pro-R)* assignment, respectively. The diastereotopic differentiation is indicated by the strength of the NOE build-up rates between *H*–C(α) and the two diastereotopic *H*–C(β) and independently verified by the interpretation of the coupling constants ^3J. For the corresponding theoretical φ angle for the different turn types, see [23b].

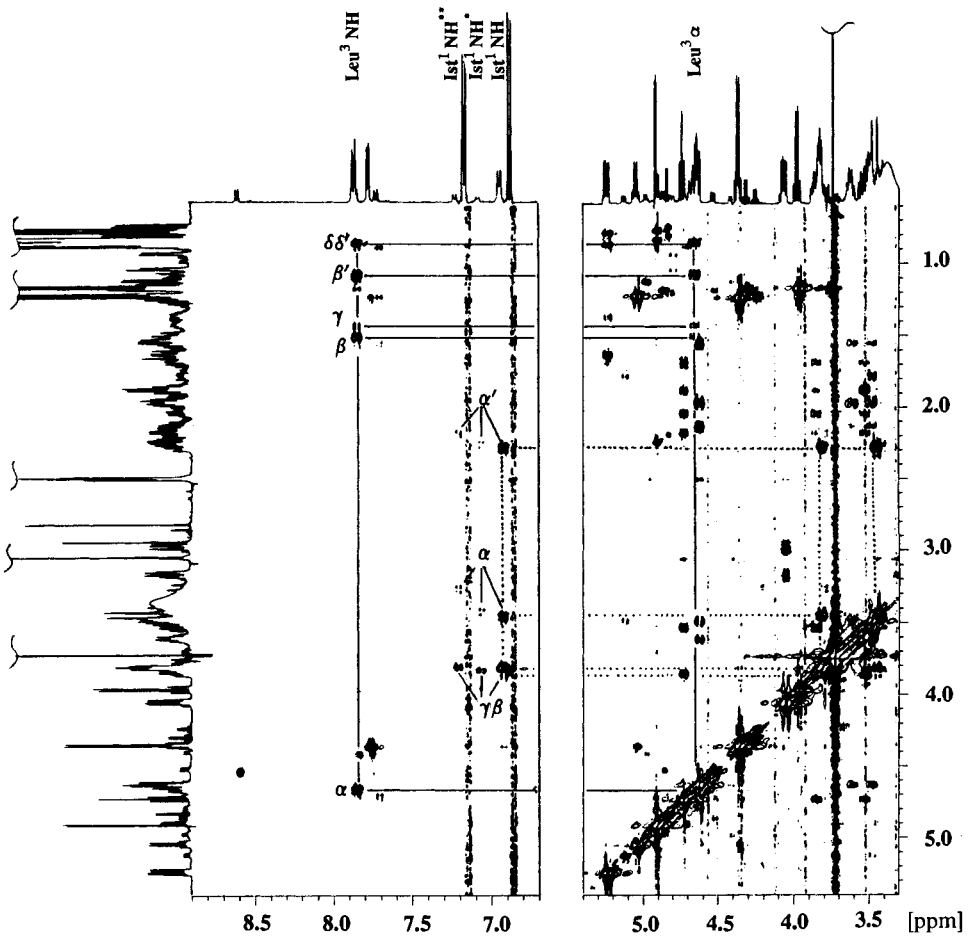

Fig. 2. *Parts of the TOCSY spectrum of didemnin B* (**2**) *in* (D_6)*DMSO solution at 300 K.* The regions of N*H* and *H*–C(α) correlations are shown. The solid lines indicate the correlations involving the Leu[3] residue, starting at N*H* and *H*–C(α). The dotted lines indicate the correlation pattern of the main conformer of Ist[1] starting at N*H* at 6.93 ppm and involving the corresponding α, β, and γ protons. Correlations to side-chain protons can be found starting at the γ proton. The assignment of the less populated conformers is pointed out (Ist[1] NH* and Ist[1] NH**).

H'–C(α) (short form: α') for each of the three detectable conformers (see *Fig. 2*). The TOCSY spectrum is also employed for the assignment of the complex spin systems of Leu, *N*-methyl-D-leucine (Me-D-Leu; short form: MeLeu), and the two Pro. The spin systems of the two minor conformers are also evident from this spectrum. As an example, the assignment of the two visible conformers of the Leu residue is given: Starting with the Leu N*H* resonance of the major conformer at 7.85 ppm, one can follow the trace to the *H*–C(α) cross-peak at 4.63 ppm, the *H*–C(β) and *H'*–C(β) (short form: β') resonances at 1.52 and 1.07 ppm, respectively, the *H*–C(γ) cross-peak at 1.44 ppm, and the degenerated *H*–C(δ) and *H'*–C(δ) (short form: δ') resonances at 0.87 ppm. Starting at the Leu N*H* resonance of the minor conformer at 7.70 ppm leads to the subsequent cross-peaks at 4.69 (*H*–C(α)), 1.55 and 1.07 (*H*–C(β) and *H'*–C(β), resp.), 1.22 (*H*–C(γ)), and finally 0.89 ppm (*H*–C(δ), *H'*–C(δ)). This procedure can also be employed starting at the *H*–C(α) or *H*–C(β) resonances.

The *N*-methyl protons of the MeLeu[7] and Me_2Tyr[5] residues are assigned with the help of an 'inverse H,C-COLOC' experiment *(Fig. 3)*. *E.g.*, the Pro[4] *C*O resonance at 170.38 ppm correlates with the Pro[4] and

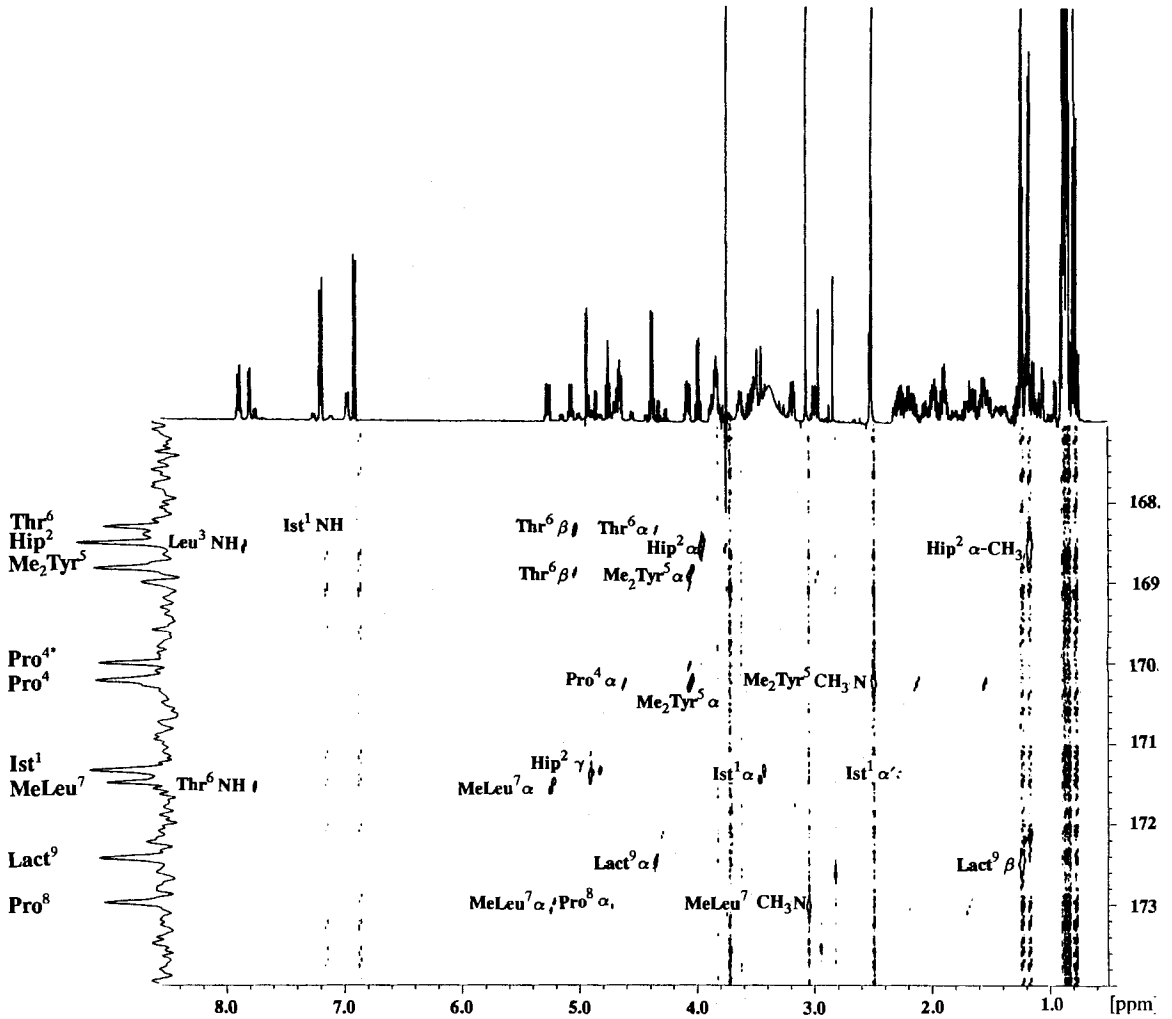

Fig. 3. *500-MHz 'inverse COLOC' spectrum with selective excitation of the carbonyl C-atoms of didemnin B* (**2**) *in* (D_6)*DMSO solution at 300 K.* The assignment of the cross-peaks and the corresponding *C*O resonances is indicated.

Me_2Tyr^5 α protons (4.62 and 4.07 ppm, resp.), the Pro^4 *H*–C(β) and *H'*–C(β) (2.14 and 1.55 ppm, resp.), and finally with the CH_3N resonance at 2.5 ppm, simultaneously providing the assignment of the Me_2Tyr^5 CH_3N group and the sequencial arrangement of Pro^4. Likewise, the Pro^8 *C*O signal at 172.9 ppm exhibits correlations to *H*–C(α), *H*–C(β), and *H'*–C(β) of Pro^8 (4.70, 2.18, and 1.67 ppm, resp.) and additionally to CH_3N and *H*–C(α) of $MeLeu^7$ (3.06 and 5.22 ppm, resp.) giving once more an independent proof of the assignment of both the CH_3N of $MeLeu^7$ and the position of the Pro^8 residue. The assignment of the remaining carbonyl C-atoms by means of the 'inverse H,C-COLOC' spectrum and the sequencing of adjacent amino-acid residues follows an analogous path, using cross-peaks to protons whose chemical shifts are already known from the DQF-COSY and TOCSY experiments. Independent proof of the sequence assignment is obtained by the NOESY experiment.

Relevant NMR Parameters for the Assignment of the Conformations of Didemnin A (1) and B (2). – The analysis of the backbone as well as of the side-chain conformation is performed by means of chemical-shift values and their temperature dependence, the

quantitative evaluation of coupling constants, and the measuring of build-up rates in NOESY spectra [23 a] with different mixing times. The limited amount of these natural products prohibits the recording of T_1 relaxation time measurements of the ^{13}C resonances as a probe of molecular flexibility.

For didemnin A (**1**), a few vicinal coupling constants are evaluated. Most of them can be obtained directly from the 1D-500-MHz ^1H-NMR spectrum or from the DQF-COSY by means of the DISCO [27] [28] technique. For didemnin B (**2**), coupling constants are

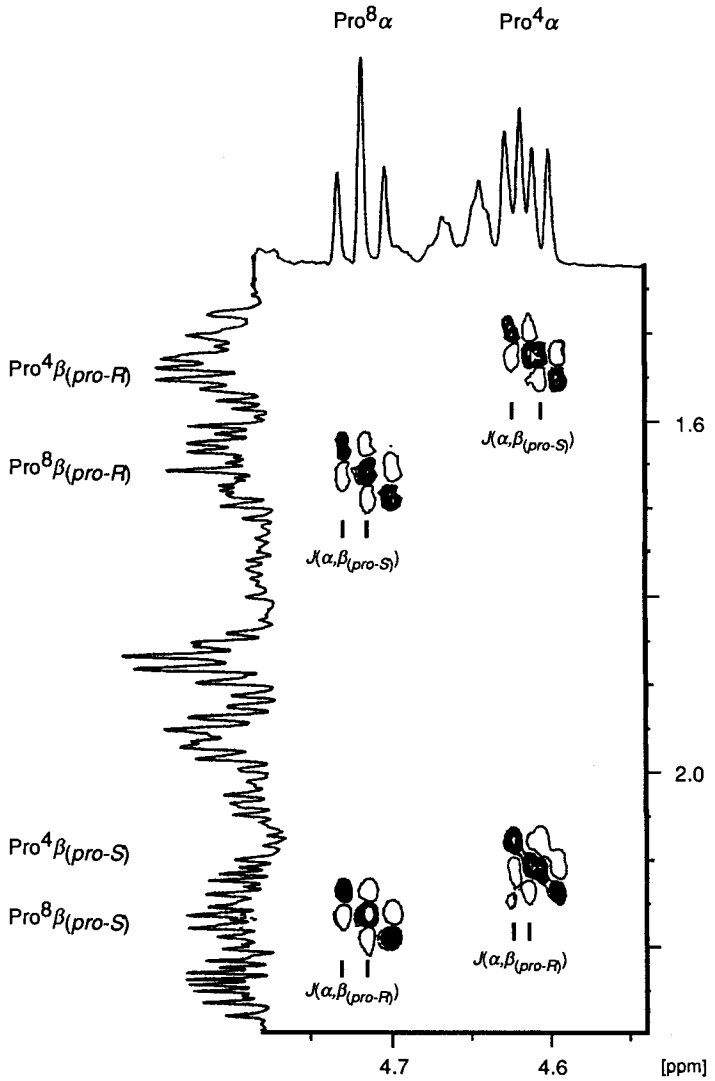

Fig. 4. *Region of the Pro⁴ and Pro⁸ α,β cross-peaks of the 500-MHz E.COSY spectrum of didemnin B* (**2**) *in (D_6)DMSO solution at 300 K.* Positive signal intensities are indicated as filled contours. The extraction of $^3J(\alpha,\beta)$ is demonstrated. For the experimental evaluation of the J, cross-sections with different F_1 frequencies are used as usual.

extracted either directly from the 1D 500-MHz ^{1}H-NMR spectrum (*e.g.* $J(NH,\alpha)$) or from an E.COSY [29] spectrum (see *Fig. 4*) which yields coupling constants with high accuracy agreeing to a large extent with those evaluated from the 1D spectrum, as far as an evaluation is possible. The E.COSY spectrum is especially suited for more complicated spin systems such as Pro and simplifies cross-peak *m* more efficiently, so that they can be analyzed by inspection.

For the determination of H...H distances, several NOESY spectra with different mixing times are recorded. Quantitative build-up rates are obtained from these experiments starting with a volume integration of the cross-peak sections and a subsequent fitting of these integrals to an exponential function after base plane correction, using the 2D-NMR program system of *Kaptein* and *Boelens* [30] on a DEC-VAX computer *(Table 2)*.

Determination of the Conformation by Molecular-Dynamics (MD) and Molecular-Mechanics (MM) Calculations. – In order to obtain reliable structural information of didemnin A (**1**) and B (**2**) in the crystalline state as well as in solution, we have performed an X-ray structure analysis of **2** [5] and the NMR studies. Additionally, we now employ MM using the program MOMO [31] and restrained MD using the GROMOS program system [32–34].

We have decided to perform only restrained dynamics and not free dynamic simulations for the following reasons. In our experience, free dynamic simulations yield artificial results due to '*in vacuo* effects' which overemphasize coulombic interactions involving additional H-bonds and sometimes even produce a misleading H-bonding pattern. *E.g.* such calculations often produce more γ turns and more bifurcated H-bonds than found by NMR and crystallographic investigations. Experimental checking *via* the recording of the temperature dependence of the NH chemical shift and specific charge release of the solvent-exposed NH protons [35] is, therefore, required. In addition, *van der Waals* interactions tend to produce a globular structure, folding side chains back close to the backbone, in contrast to the NMR findings. An example of this effect has been found in cyclo (-D-Pro-Phe-Thr-Lys(Z)-Trp-Phe-) [35] where in a free dynamic simulation, the Trp indole moiety occupies conformation $\chi_1 = 60°$, in contrast to the information from the homo- and heteronuclear coupling constants *J* which lead to a population of less than 10% for this rotamer. Similar observations have been made for the Me-Bmt side chain in cyclosporin A [36]. Hence, a free dynamic calculation of molecules of this size do not yield structures independent of the starting structure, and the calculated conformations are not in good agreement with detailed experimental observations.

It might be better to calculate molecules *in solution,* but the tremendous computer CPU time required for the calculation of a sufficiently long trajectory (the viscosity of the solvent slows down the dynamics!) prevents this application in realistic cases, but in general, efforts should be made to parametrize the force field for the solvents in which the NMR spectra are recorded.

We will now focus on the conformation of **1** and **2** in solution. For this purpose, we use two different approaches, each of which starting with the crystal coordinates of **2** [5]. First, we employ MOMO, a low-cost molecular-modeling program system based on force-field techniques. Secondly, we perfom restraint MD simulations using the GROMOS package. The results of the two approaches will be compared to demonstrate the reliability of the MM approach using MOMO.

Table 2. *Comparison of Experimental and Calculated H...H Distances* r [pm] *for Didemnin B* (**2**) *and A* (**1**) *Obtained from NOE Build-up Rates, Molecular-Dynamics, and Molecular-Mechanics Calculations*[a])

	Involved protons		$r(H,H)^{NOE}$	$r(H,H)^{CRYST}$	$r(H,H)^{MD-R}$	$r(H,H)^{MD}$	$r(H,H)^{MM-R}$	$r(H,H)^{MM}$
2	Ist[1] NH	Ist[1] H–C(γ)	231	299	208	204	243	303
	Ist[1] NH	Ist[1] $H_{(pro\text{-}S)}$–C(α)	252	286	268	313	252	301
	Ist[1] NH	Pro[4] H–C(α)	339	331	348	373	339	319
	Ist[1] NH	Thr[6] H–C(α)	210	223	209	198	210	225
	Ist[1] H–C(γ)	Ist[1] H–C(δ)	210	247	237	239	221	238
	Ist[1] H–C(γ)	Ist[1] $H_{(pro\text{-}S)}$–C(α)	231	283	273	278	236	290
	Ist[1] H–C(δ)	Ist[1] H–C(ε)	257	242	266	266	257	246
	Ist[1] $H_{(pro\text{-}S)}$–C(α)	Leu[3] NH	264	264	298	373	274	304
	Hip[2] H–C(γ)	Hip[2] H–C(δ)	255	243	233	278	255	248
	Hip[2] H–C(γ)	Hip[2] H–C(α)	363	335	347	350	363	373
	Hip[2] H–C(γ)	Hip[2] CH_3–C(α)	346	441	482	478	356	483
	Hip[2] H–C(γ)	Hip[2] CH_3(ε)	283	299	302	337	293	325
	Hip[2] H–C(α)	Leu[3] NH	200	214	215	219	211	230
	Leu[3] NH	Leu[3] H–C(α)	301	301	289	289	303	301
	Leu[3] NH	Thr[6] H–C(α)	324	326	327	324	334	292
	Leu[3] NH	MeLeu H–C(α)	306	402	351	363	317	408
	Leu[3] H–C(α)	Leu[3] $H'_{(pro\text{-}R)}$–C(β)	290	303	302	303	300	304
	Leu[3] H–C(α)	Leu[3] $H_{(pro\text{-}S)}$–C(β)	240	253	263	261	250	244
	Leu[3] H–C(α)	Leu[3] CH_3(ε)	226	203	315	312	226	243
	Leu[3] $H_{(pro\text{-}R)}$–C(β)	Leu[3] H–C(γ)	231	253	258	258	241	250
	Leu[3] $H_{(pro\text{-}S)}$–C(β)	Pro[4] H–C(β)	309	330	342	348	319	388
	Leu[3] $H_{(pro\text{-}R)}$–C(β)	Thr[6] H–C(α)	257	279	278	321	257	206
	Leu[3] $H_{(pro\text{-}S)}$–C(β)	Thr[6] H–C(α)	316	381	351	411	326	365
	Pro[4] H–C(α)	Me_2Tyr[5] CH_3N	192	193	252	251	202	235
	Pro[4] $H_{(pro\text{-}R)}$–C(β)	Me_2Tyr[5] CH_3N	246	245	379	412	256	241
	Me_2Tyr[5] CH_3N	Me_2Tyr[5] H–C(α)	204	239	261	259	210	203
	Me_2Tyr[5] H–C(α)	Me_2Tyr[5] $H_{(pro\text{-}S)}$–C(β)	234	234	248	249	238	236
	Thr[6] NH	Thr[6] H–C(α)	276	289	264	275	276	288
	Thr[6] NH	Thr[6] H–C(β)	229	232	222	237	239	243
	Thr[6] NH	Pro[8] H–C(α)	353	375	415	462	353	353
	Thr[6] NH	MeLeu[7] H–C(α)	261	301	300	341	261	279
	Thr[6] H–C(α)	Thr[6] H–C(β)	243	257	257	256	243	248
	MeLeu[7] CH_3N	MeLeu[7] H–C(α)	286	369	370	366	298	368
	MeLeu[7] CH_3N	Thr[6] NH	260	251	306	286	260	280

	MeLeu^7 CH_3N	Pro^8 H–C(α)	286	316	280	288	296	241
	MeLeu^7 H–C(α)	MeLeu^7 $H_{(pro\text{-}R)}$–C(β)	233	246	267	276	243	246
	MeLeu^7 H–C(β)	MeLeu^7 H–C(γ)	237	247	284	263	247	257
	MeLeu^7 H–C(α)	MeLeu^7 CH_3(δ)	249	204	376	332	249	236
	MeLeu^7 H–C(α)	MeLeu^7 CH_3(δ′)	295	435	381	412	–	–
	Pro^8 H–C(δ)	Lact^9 H–C(α)	247	224	221	216	257	269
1	Ist^1 NH	Ist^1 H–C(γ)	238	–	281	290	249	300
	Ist^1 NH	Thr^6 H–C(α)	215	–	212	204	215	229
	Ist^1 NH	Ist^1 CH_3–C(δ)	256	–	331	303	266	251
	Ist^1 NH	Ist^1 $H_{(pro\text{-}S)}$–C(α)	266	–	258	292	266	265
	Ist^1 OH	Ist^1 H–C(δ)	267	–	295	318	277	340
	Ist^1 OH	Ist^1 H–C(β)	232	–	228	248	243	235
	Ist^1 OH	Ist^1 $H_{(pro\text{-}S)}$–C(α)	299	–	284	256	310	360
	Hip^2 H–C(α)	Hip^2 H–C(γ)	351	–	344	347	355	377
	Hip^2 H–C(γ)	Hip^2 H–C(δ)	260	–	237	230	260	250
	Leu^3 NH	Thr^6 H–C(α)	320	–				
	Leu^3 NH	Ist^1 $H_{(pro\text{-}S)}$–C(α)	279	–	310	365	289	281
	Leu^3 NH	Hip^2 H–C(α)	218	–	212	215	218	233
	Leu^3 NH	Hip^2 CH_3–C(α)	318	–	373	366	328	339
	Leu^3 NH	Leu^3 H–C(α)	302	–	289	288	303	300
	Leu^3 NH	Leu^3 $H_{(pro\text{-}R)}$–C(β)	275	–	257	244	275	263
	Leu^3 H–C(α)	Leu^3 $H_{(pro\text{-}R)}$–C(β)	311	–	303	304	311	303
	Leu^3 H–C(α)	Leu^3 $H_{(pro\text{-}S)}$–C(β)	252	–	255	260	252	240
	Leu^3 H–C(α)	Pro^4 H–C(δ)	262/210	–	243	239	220	284
	Pro^4 H–C(α)	Ist^1CH_3–C(δ)	273	–	343	299	283	310
	Pro^4 H–C(α)	Me_2Tyr^5 CH_3N	204	–	247	258	212	245
	Me_2Tyr^5 H–C(α)	Me_2Tyr^5CH_3N	216	–	256	261	216	202
	Thr^6 H–C(α)	Ist^1 $H_{(pro\text{-}S)}$–C(α)	331	–	319	359	341	358
	Thr^6 NH	Thr^6 H–C(α)	310	–	281	282	309	299
	Thr^6 NH	Thr^6 H–C(β)	279	–	340	271	290	249
	Thr^6 NH	Thr^6 H–C(γ)	273	–	330	395	273	240
	Thr^6 NH	Ist^1 H–C(γ)	262	–	338	527	272	502
	Thr^6 NH	Ist^1 $H_{(pro\text{-}S)}$–C(α)	283	–	309	446	294	477
	Thr^6 H–C(α)	Thr^6 H–C(β)	251	–	238	247	251	255
	MeLeu^7 CH_3N	Ist^1 $H_{(pro\text{-}S)}$–C(α)	330	–	334	524	330	276

[a]) CRYST, crystal structure of **2**; MD-R, averaged conformation, obtained after 70-ps restrained MD calculations *(in vacuo)*; MD, subsequent 30-ps unrestrained MD simulation *(in vacuo)*; MM-R, conformation obtained after a restrained MOMO calculation; MM, subsequent unrestrained energy minimization with MOMO.

MOMO is an interactive modeling system with graphics capabilities which we use on personal computers (PC) and DEC-VAX computers. It implements the force-field and π-SCF algorithm of PIMM (written by *Lindner* [37]) with extensions for hetero atoms (O, N, F, Cl, bivalent S) and atomic charges [38]. Electrostatic interactions are treated by a point-charge model with charges calculated by the method of *Marsilli* and *Gasteiger* [39] for the σ-system and π-charge densities from the π-SCF calculations. For the calculation of the solution conformation incorporating the experimental intramolecular distances, we introduce an additional potential function $E_{restraint}$:

$$E_{restraint} = \begin{cases} k\,(r\text{-}r_{min})^2 & \text{for } r < r_{min} \\ k\,(r\text{-}r_{max})^2 & \text{for } r > r_{max} \\ 0 & \text{for } r_{min} < r < r_{max} \end{cases}$$

with k = force constant (kJ · mol^{-1} · Å^{-2}), r_{min} = estimated distance lower limit (from NOE measurements), r_{max} = estimated distance upper limit, and $r_{min} < r_{max}$. With this restrained MM calculation, we generate a starting conformation for a subsequent unrestrained MM calculation (assuming that the differences between hypothetical gas-phase structures and solution structures are not too large). The force constant k is used for weighting the experimental observations. This splitting of the potential function into three parts is used to accommodate for uncertain experimental distances, especially for those concerning (rotating) methyl protons. However, this approach can be described as a kind of a 'distance geometry' approach to get an image of the structure and to reach a maximum of consistency with the experimental data (see *Table 3*).

Table 3. *Characteristic Data of Different MOMO Calculations for Didemnin B* (**2**) *and A* (**1**)[a])

	$\pi\Delta$[E-5]	rms shift [E-6]	rms grad	E.o.D	ΔH_f
2, X-ray	0.19	0.035	0.009	−2938	−3411
2, MM-R	0.24	0.023	0.017	−2812	−3394
2, MM	0.27	0.021	0.004	−2938	−3413
2, MD-RS[b])	0.37	0.030	0.009	−2793	−3382
1, X-ray[c])	0.00	0.000	0.001	−2482	−2826
1, MM-R	0.40	0.167	0.002	−2179	−2737
1, MM	0.21	0.067	0.001	−2261	−2801
1, MD-RS[b])	0.45	0.017	0.003	−2361	−2825

[a]) Other calculations, see *Tab. 2*.
[b]) Calculation starts from a low-energy conformation of the specified MD calculation.
[c]) Starting coordinates are derived from the X-ray structure of **2**.

The GROMOS MD simulations [34] involve the calculation of trajectories of a system containing N atoms, solving *Newton*'s equations of motion for each atom by the integration of the $3N$ coupled differential equations using small time steps. The total energy of this system is composed of the kinetic and the potential energy of all N atoms. If one would like to perform MD simulations at *e.g.* a constant temperature, a coupling of the systems of N atoms to an external temperature bath must take place. The strength of the coupling to this bath is controlled by a temperature relaxation time [40]. The empirical energy function employed includes terms accounting for covalent-bond stretching, bond-angle bending, harmonic dihedral bending, sinusoidal dihedral torsion, *van der Waals*

and electrostatic interactions, and an additional potential term to satisfy a set of distance restraints. Special terms for H-bond interactions are not necessary because of the description of those forces by the *van der Waals* and *Coulomb* potentials. The force-field employed is parameterized especially for peptides and nucleic acids. The starting coordinates are taken from the crystal structure of **2** [5]. The initial structure is relaxed by performing 500 conjugate gradient energy-minimization (EM) steps [41].

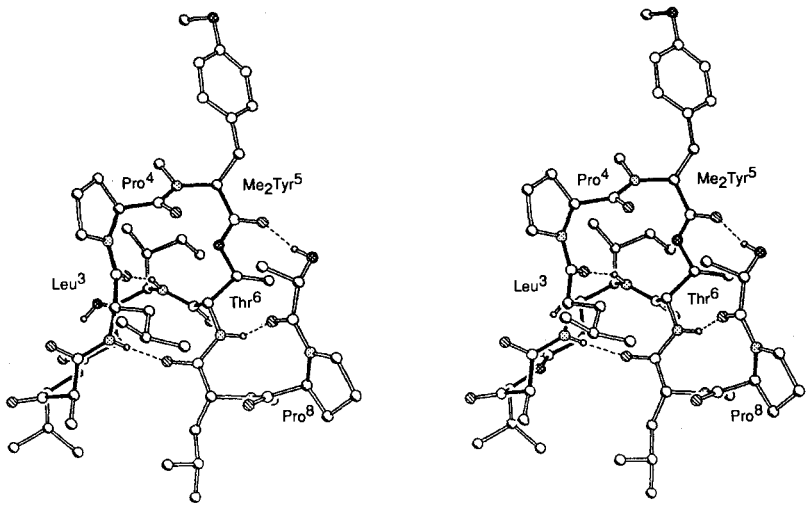

Fig. 5. *Stereoview of the trajectory* (mean conformation) *of didemnin B* (**2**) *obtained by 70-ps restrained MD calculation* (*in vacuo*)

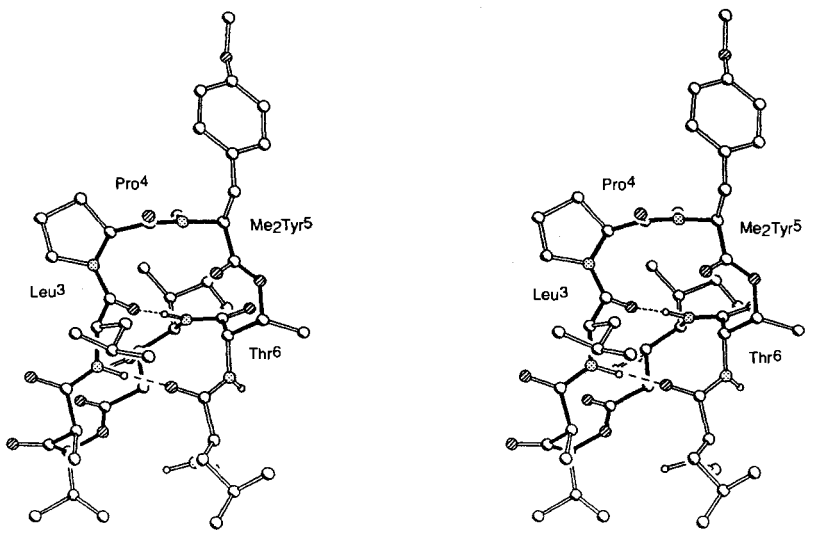

Fig. 6. *Stereoview of the trajectory* (mean conformation) *of didemnin A* (**1**) *obtained by 70-ps restrained MD calculation* (*in vacuo*)

A 100-ps MD run is started for both **1** and **2** each of which being split into two parts. During the first 70 ps, the experimentally obtained distance restraints (force constant $K_{dc} = 2000\ kJ \cdot mol^{-1} \cdot nm^{-2}$) are included, using the first 10 ps for the equilibration of the molecule. In order to overcome potential-energy barriers of the order of the magnitude of a H-bond, a starting temperature of 1000 K is chosen. This initial temperature is then lowered stepwise to 300 K from the 1st to the 5th ps of the simulation. The period from 11 ps to 70 ps is used for averaging. During the last 30 ps, a free MD simulation is performed to prove the stability of the 'restraint low-energy conformation' and to extract information of the flexibility of the molecule as far as possible. The results are given in *Figs. 5* and *6*.

Conformation of Didemnin B (2) in the Crystalline and Solution State. – While performing conformational analysis, it is important to know whether there is conformational homogeneity [18] [42] [43] on the time-scale of the experiments or not. The appearence of only one set of signals leads to the decision that there is no conformational equilibrium involving a barrier of more than 60 kJ/mol, indicating for example a *cis/trans* isomerism about an amide bond, but this finding does not exclude fast-interconverting conformations. Although there are several criteria indicating a preferred conformation, an equilibrium might also be detected by the disagreement of observed and calculated intramolecular distances obtained from NOE values [44], nowadays best detected in the course of restraint MD calculations [35]. Usually, the most stringent way to test conformational homogeneity is an examination with the assistance of molecular-modeling techniques. The internal consistency of the experimentally observed data (*e.g.* NOE's, coupling constants, and temperature gradients of NH protons) with a structure which does not violate expected conformational features, *e.g.* usual turn patterns [45–47], gives a strong indication of conformational homogeneity and also shows that the results of the

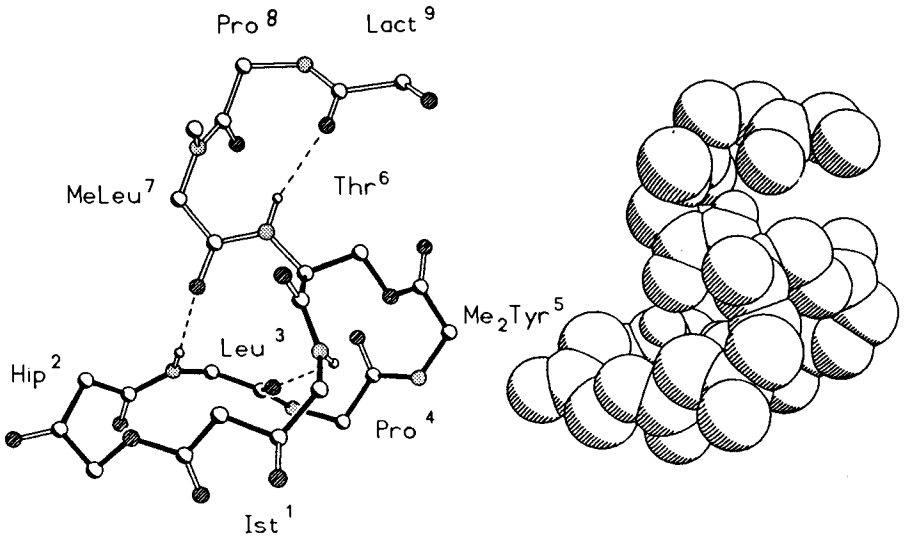

Fig. 7. *Ball-and-stick and space-filling drawings of the backbone of the crystal structure of didemnin B* (**2**) [5] *showing the intramolecular H-bond pattern and the bent 'figure-of-eight' folding of the macrocyclic ring.* The same orientation is chosen for both representations.

conformational analysis are reliable. In our case, we observe three signal patterns in the spectra of didemnin B (**2**) in (D_6)DMSO solution, but only for a distinct part of the molecule. The major conformer is the only one showing sufficient conformationally relevant NMR parameters.

The most important conformational features of the crystal structure of **2** [5] are now compared to the calculated structure in solution. In the solid state, the 23-membered ring of **2** is folded like a bent 'figure-of-eight' (see *Fig. 7*) and stabilized by one transannular H-bond linking the Ist[1] amide group with the Leu[3] carbonyl O-atom, forming a bridge across the middle of the macrocyclic ring. A similar H-bonding pattern is indicated for **2** in solution by a temperature dependence of the chemical shift of the Ist[1] N*H* which indicates an intramolecular H-bond (see *Table 4* for the $-\Delta\delta/\Delta T$ quotients and *Table 5* for the experimental and calculated donor-acceptor distances for the different types of H-bridges). A possible cause for the irregular shape of the backbone might be the H-bond linking the Leu[3] amide group to the MeLeu[7] carbonyl group, folding the linear moiety (MeLeu[7], Pro[8], Lact[9]) back to the macrocyclic system (see *Fig. 7* for the H-bond pattern).

Table 4. *Temperature Dependence of the* N*H Chemical Shifts of* **1** *and* **2**, *Given as* $-\Delta\delta/\Delta T$ [ppb/K]

	Ist[1]	Leu[3]	Thr[6]
$-\Delta\delta/\Delta T$ for **1**	4.0	1.5	6.4
$-\Delta\delta/\Delta T$ for **2**	0.5	1.8	4.3

Once more, the $-\Delta\delta/\Delta T$ quotients *(Table 4)* indicate an internal orientation of the Leu[3] N*H*, most likely to form an intramolecular H-bridge to the MeLeu[7] C*O*. According to the donor-acceptor distance, this H-bridge is the strongest in the crystal structure, and it is also found to be very strong (100% occupancy) in solution, according to the different conformational calculations (see *Table 5*).

The third H-bond apparent in the crystalline state of **2** is involved in a βII structure for the linear side chain with Pro[8] in the $(i + 1)$ position, a preferred position for proline in β turns [47], and MeLeu[7] in the $(i + 2)$ position. A similar structure in solution is indicated by the NOE between Thr[6] N*H* and Pro[8] *H*–C(α) with a H...H distance of 353 pm, the relative strong NOE between Pro[8] *H*–C(α) and MeLeu[7] C*H*$_3$N (286 pm compared with *ca.* 320 pm in the crystal structure; see *Table 2*), and the strong NOE between MeLeu[7] C*H*$_3$N and Thr[6] N*H* (260 pm). This structural feature is well reproduced by all conformational calculations (see *Table 6* for the ideal and experimentally observed dihedral angles). However, the GROMOS simulations reveal an additional H-bridge linking the Lact[9] OH with the Me$_2$Tyr[5] CO group (see *Table 5*), stabilizing the side-chain arrangement. This feature is not found in the crystal structure (the lactoylproline moiety is disordered) and is also not duplicated in the MOMO calculations.

There are two more βII turns observed in the macrocyclic system of didemnin B (**2**), which are unconventional because there is no possibility of H-bridge formation, but which are classical βII turns in terms of their geometry. This is surprizing and supports earlier observations that the formation of a H-bridge is not essential for a specific turn structure [48]. A third turn involving the Hip[2] residue on its own cannot be assigned to any classical turn type.

The first unconventional βII structure involves the Thr[6] residue in $(i + 1)$ and the Ist[1] residue in the $(i + 2)$ positions. The observed geometry (see *e.g. Fig. 7*) can be described

Table 5. *H-Bonds*[a]) *in Didemnin A* (**1**) *and B* (**2**). Comparison of the values of the different calculations[b]).

	Donor Ist[1] N*H*		Acceptor Leu[3] C*O*	Donor Leu[3] N*H*		Acceptor MeLeu[7] C*O*	Donor Thr[6] N*H*		Acceptor Lact[9] C*O*	Donor Lact[9] O*H*		Acceptor Me_2Tyr[5] C*O*
	r[pm][c])	*Θ*[deg][d])	*P*[%][e])	*r*[pm][c])	*Θ*[deg][d])	*P*[%][e])	*r*[pm][c])	*Θ*[deg][d])	*P*[%][e])	*r*[pm][c])	*Θ*[deg][d])	*P*[%][e])
2, CRYST	302	142	–	291	169	–	309	156	–	433[f])	–	–
2, MM-R	275	173	–	281	159	–	268	177	–	–	–	–
2, MM	273	152	–	265	169	–	270	175	–	–	–	–
2, MD-R	280	158	99	290	162	100	289	152	96	296	159	90
2, MD	281	157	98	283	157	100	303	146	42	288	161	98
1, MM-R	302	153	–	265	156	–						
1, MM	279	147	–	266	166	–						
1, MD-R	289	159	100	279	160	100						
1, MD	289	160	99	289	159	99						

	Donor MeLeu[7] N*H*		Acceptor Ist[1] *Q*(ester)
	r[pm][c])	*Θ*[deg][d])	*P*[%][e])
1, MD	340	140	47
1, MD	–	–	–

[a]) Definition of H-bridge bonds: D–H...A is shorter than 300 pm and the corresponding H angle is greater than 120° (D = donor, A = acceptor).

[b]) Explanation of the codes for the different calculations, see *Table 2*.

[c]) Distances between D–H.

[d]) Angle between (D–H... A).

[e]) Population of the H-bridge during the MD calculations.

[f]) This H-bridge is not appearent in the crystal structure, see *Fig. 7*.

best by a turn of the βII type, although the differences of the observed dihedral angles from those ideally expected is fairly high (up to 60°, see *Table 6* and *Fig. 8*). The following NMR evidence supports this conclusion. Firstly, the H-bridge between Leu[3] NH and MeLeu[7] CO, responsible for the folding back of the linear moiety to the macrocyclic ring, indicated by a strong NOE between Leu[3] N*H*, and Ist[1] $H_{(pro\text{-}S)}$–C(δ) (264 pm, see *Table 2*) strengthen the assumption of a turn structure. Secondly, the NOE between Ist[1] *H*–C(γ) and Ist[1] $H_{(pro\text{-}S)}$–C(α) (231 pm; a coupling constant $^3J(\alpha,\beta)$ cannot be extracted) and the coupling constant $^3J(\mathrm{NH},\gamma) = 9.7$ Hz points to a $(i+2)$ position for Ist[1] in a pseudo-βII turn. At least the strong NOE between Ist[1] N*H* and Thr[6] *H*–C(α) (210 pm) and the small $^3J(\alpha,\mathrm{NH})$ (5.7 Hz) do not contradict the assumption of Thr[6] being involved in the $(i+1)$ position of a βII turn. The observed $^3J(\alpha,\beta)$ (2.4 Hz) for Thr[6] agrees well with the *H*–C(α)–C(β)–*H* torsion angle in the crystal (79.4°). Again, this structure is reproduced fairly well in the different conformational simulations (see *Tables 2* and *6*) and remains close to the crystal structure with a maximum deviation of *ca.* 40° for the torsional angles (see *Table 6* and *Fig. 8* for the corresponding *Ramachandran* plots).

Table 6. *Comparison of Topologically Relevant Dihedral Angles in Didemnin B* (**2**) *and A* (**1**)

a) Indication of a βII Turn in the Linear Peptide Chain of **2**, *Including Pro[8] and MeLeu[7]*

	Pro[8]		MeLeu[7]	
	φ	ψ	φ	ψ
2, IDEAL	–60	120	80	0
2, CRYST	–63	124	103	–29
2, MM-R	–50	133	96	–38
2, MM	–45	120	123	–49
2, MD-R	–53	120	112	–18
2, MD	–60	116	96	27
2, MD-RS[b])	–65	127	107	–12

b) Indication of an Unconventional βII Turn in the Macrocyclic Ring of **2**, *Including Thr[6] and Ist[6]*

	Thr[6]		Ist[1]	
	φ	ψ	φ	ψ
2, IDEAL	–60	120	80	0
2, CRYST	–68	156	113	–58
2, MM-R	–51	123	147	–76
2, MM	–64	142	106	–62
2, MD-R	–48	121	122	–60
2, MD	–76	119	123	–70

c) Indication of an Unconventional βII Turn in the Macrocyclic Ring of **1**, *Including Thr[6] and Ist[1]*

	Thr[6]		Ist[1]	
	φ	ψ	φ	ψ
1, IDEAL	–60	120	80	0
1, MM-F[c])	–73	141	109	–62
1, MM-R	–163	89	140	–95
1, MM	–76	126	131	–61
1, MD-R	–123	81	141	–60
1, MD	–79	112	123	–63
1, MD-RS[b])	–128	83	137	–64

Table 6 (cont.)

d) Indication of an Unconventional βII Turn in the Macrocyclic Ring of **2**, *Including Pro*$^+$ *and* Me_2Tyr^5

	Pro^4		Me_2Tyr^5	
	ϕ	ψ	ϕ	ψ
2, IDEAL	–60	120	80	0
2, CRYST	–75	163	51	40
2, MM-R	–81	156	57	25
2, MM	–72	162	60	15
2, MD-R	–68	149	52	56
2, MD	–60	146	46	65
2, MD-RS[b])	–69	139	56	60

e) Indication of an Unconventional βII Turn in the Macrocyclic Ring of **1**, *Including* Pro^4 *and* Me_2Tyr^5

	Pro^4		Me_2Tyr^5	
	ϕ	ψ	ϕ	ψ
1, IDEAL	–60	120	80	0
1, MM-F[c])	–70	161	60	16
1, MM-R	–55	162	91	–86
1, MM	–49	165	62	–114
1, MD-R	–66	126	68	109
1, MD	–63	128	59	96

[a]) Explanation of the calculations, see *Table 2*. [b]) Low-energy conformation of the specified MD calculation. [c]) Free MM calculation of **1**, starting from X-ray coordinates.

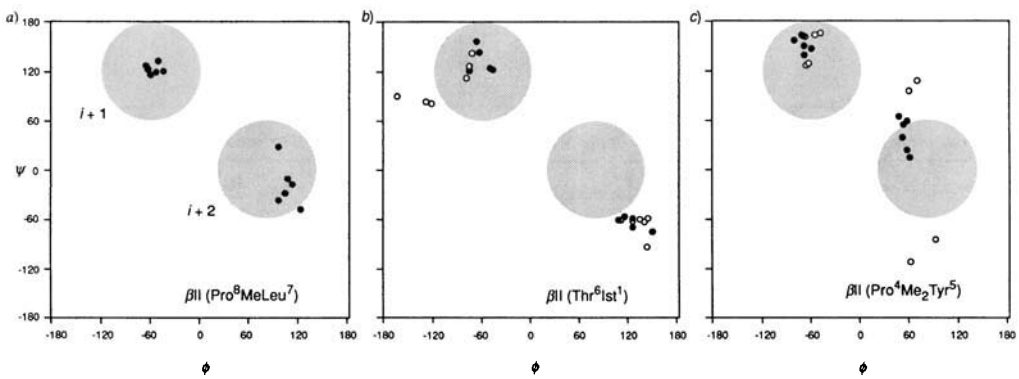

Fig. 8. Ramachandran *diagram of the turns* (ϕ and ψ angles) *in didemnins*. Filled circles indicate conformations of didemnin B (**2**) and open circles of didemnin A (**1**). The different points correspond to the different calculations shown in *Table 6*. a) *βII* Turn in the linear side chain of **2** with Pro^8 in the ($i + 1$) position and $MeLeu^7$ in the ($i + 2$) position. b) Turn involving Thr^6 and Ist^1 in **1** and **2**, indicating that the amino acids occupy a βII-turn-like structure with these residues in $i + 1$ and $i + 2$ position. An H-bond cannot be formed due to the lack of H-bond donor in $i + 3$ position. c) Turn about Pro^4 and Me^2Tyr^5 in **1** and **2** (argumentation similar to *b*). Two MOMO-derived structures in **1** deviate in the ψ angle in position $i + 2$.

The second unconventional βII turn involves the Pro^4 residue in the expected ($i + 1$) position and the Me_2Tyr^5 residue in the ($i + 2$) position. Again, the usual H-bond donor and acceptor atoms are involved, but with a lactone instead of an amide bond between Me_2Tyr^5 in the ($i + 2$) and Thr^6 in the ($i + 3$) positions. Again, no conformationally

Table 7. *Results of Selected Least-Squares Fits Involving the Backbone Atoms of the Macrocyclic System of Didemnin A* (**1**) *and B* (**2**)[a]). For some related calculations, see *Table 2*. R.m.s. deviations are given in Å.

		CRYST	MD-R	MD	MM-R	MM
2	CRYST	–	0.40	0.57	0.28	0.46
	MD-R	–	–	0.23	0.47	–
	MD	–	–	–	–	0.32
	MM-R	–	–	–	–	0.52
1	CRYST	–	1.01	0.71	0.70	0.43
	MD-R	–	–	1.64	0.62	–
	MD	–	–	–	–	0.88
	MM-R	–	–	–	–	0.55

[a]) Explanation of the calculations, see *Table 2*.

relevant coupling constants can be extracted (*e.g.* because of the methylation of the Me_2Tyr^5 amide N-atom) to confirm our assumption. However, the NOE pattern does not contradict our assumption that in (D_6)DMSO solution, the same type of pseudo-βII turn is formed as in the crystalline state. There is a strong NOE between Me_2Tyr^5 CH_3N and Me_2Tyr^5 H–C(α) (204 pm) and a strong NOE between Me_2Tyr^5 CH_3N and Pro^4 H–C(α), (192 pm) pointing to a βII *versus* a βII' turn. The strongest indications of a turn structure in this part of the molecule are the observed NOE between Ist^1 NH and Pro^4 H–C(α) (339 pm) and Leu^3 NH and Ist^1 $H_{(pro\text{-}S)}$–C(α) (264 pm), indicating a close contact of the (i) and ($i + 4$) positions. Once more, the observed NOE's fit well to distances observed in the crystal structure (see *Table 2*), and the distance-restrained modeled structures remain fairly close to the crystal structure (see *Table 6* for the relevant dihedral angles and *Fig. 8* for the corresponding *Ramachandran* plots). We have performed least-squares fits of the 23-membered ring backbone atoms, for each pair of structures (see *Table 7*) showing the

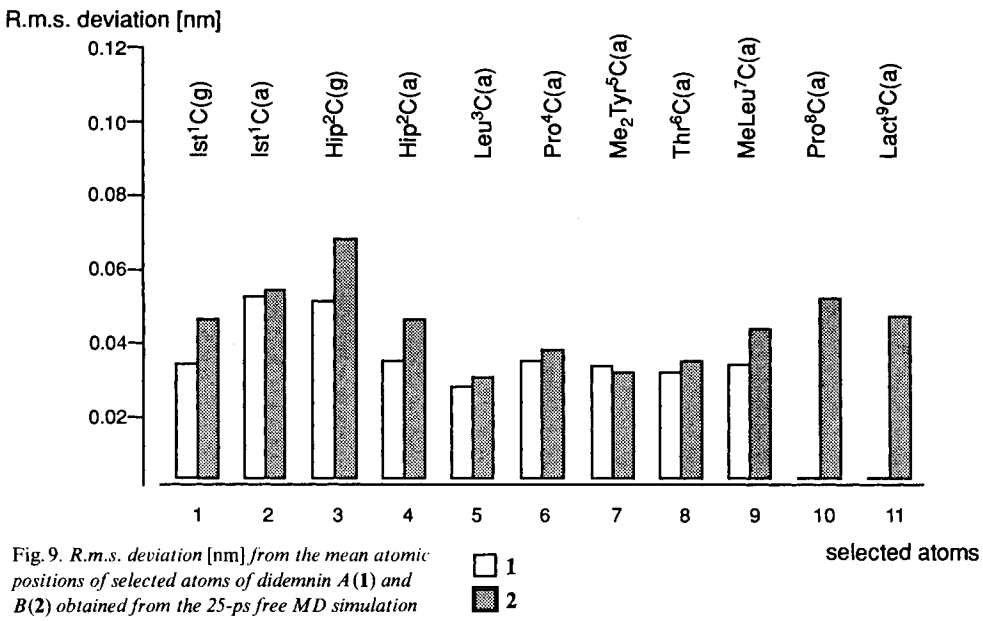

Fig. 9. *R.m.s. deviation* [nm] *from the mean atomic positions of selected atoms of didemnin A* (**1**) *and B* (**2**) *obtained from the 25-ps free MD simulation*

near equivalence of the crystal and calculated solution structures. The overall r.m.s. for the positional fluctuation of selected backbone atoms during the analyzed 25 ps free MD simulations seem to be sufficiently low (see *Fig. 9*) to describe the macrocyclic system as fairly rigid. There are minor exceptions in the region of the Hip[2] residue which does not show any intramolecular H-bonding requiring structural rigidity. As expected, higher fluctuations are observed for the atoms involved in the linear moiety.

Conformation of the Side Chains. – In general, side chains are more flexible than the backbone, and conformational homogeneity should not be expected. The assignment of the side-chain rotamers about the C(α)–C(β) bond (χ_1) [49] seems only reasonable if one of the three staggered conformations is dominant in the equilibrium.

The method applied to the conformational analysis of side chains follows a published procedure [50]. First, the vicinal homonuclear coupling constants $^3J(\alpha,\beta)$ and $^3J(\alpha,\beta')$ are taken into account, if available. This allows to decide between conformations **I** ($\chi_1 = -60°$) and **II** ($\chi_1 = 180°$) on the one hand and **III** ($\chi_1 = +60°$) on the other hand (signs of χ_1 for an L-amino acid). If one of the conformations **I** or **II** dominates, the assignment of the diastereotopic protons of the *ABX* system is done on the basis of NOEs and heteronuclear $^3J(C',H–C(\beta))$ coupling, using the COLOC technique [50].

Starting with Ist[1] which can be described as a pseudo-D-amino acid, we find conformation **I** in the crystalline state of **2** ($\chi_1 = 64.2°$). Unfortunately, $^3J(\gamma,\delta)$ can neither be extracted out of the 1D spectrum due to strong overlap at 3.8 and 1.87 ppm, respectively, nor out of the E.COSY spectrum because of the severe overlap of the H–C(γ) and H–C(β) resonances (3.82 and 3.80 ppm, resp.). Applying the NOE between Ist[1] H–C(γ) and Ist[1] H–C(δ) (210 pm) as restraint to the side chain of Ist[1], the staggered conformation **I** is retained during all the different conformational calculations starting from the crystal structure (see *Table 8*).

For the Hip[2] residue containing two diastereotopic Me groups instead of diastereotopic protons, conformation **III** ($\chi_1 = 60°$); χ_1 relative to $Me_{(pro\text{-}R)}$ is present in the crystal structure. The $^3J(\gamma,\delta)$ 3.9 Hz favors a predominance of conformation **I** and **III**. Using

Table 8. *Dihedral Angles* χ_1 [°] *Didemnin B* (**2**) *and A* (**1**)[a])

	Ist[1]	Leu[3]	Me_2Tyr[5]	Thr[6]	MeLeu[7]
2, CRYST	64.2	–66.8	–41.8	–154.5	60.7
2, MM-R	47	–69	–43	–165	47
2, MM	53	–50	–42	–156	61
2, MD-RS[b])	61	–72	–63	–156	80
2, MD-R	64	–72	–62	–153	74
2, MD	64	–74	–63	–162	135
2, MD-RS2[b])	52	–78	–70	–165	87
1, MM-F[c])	52	–51	–40	–161	56
1, MM-R	72	–59	–40	–150	60
1, MM	68	–48	–44	–144	64
1, MD-RS[b])	71	–65	–67	–178	–179
1, MD-R	73	–61	–66	–179	91
1, MD	64	–70	–66	–170	69

[a]) Explanation of the different calculations, see *Table 2*.
[b]) Low-energy structure of the restraint MD calculations.
[c]) Free MOMO calculation of **1** starting with coordinates obtained from the X-ray structure of **2**.

Pachler's equations [51–53], the population of rotamer **II** is *ca.* 12%, whereas rotamer **I** or **III** are populated up to 88% (e.s.d. *ca.* 10%). There is no unambiguous evidence for a discrimination between rotamers **I** and **III**. In the crystal structure, the $Me_{(pro\text{-}R)}$ group is located a bit closer to the ketone moiety of Hip[2] which might account for the slight downfield shift (0.83 *vs.* 0.76 ppm) of one of the Me resonances. This observation would favor rotamer **III** in solution too.

In the crystal structure of didemnin B (**2**), the Leu[3] residue adopts conformation **I** ($\chi_1 = -66.8°$). Despite of the lack of homonuclear coupling information (the cross-peaks are situated in a crowded region of the E.COSY spectrum), the assignment of the diastereotopic β protons is possible by means of NOE's. So, $H_{(pro\text{-}S)}$ *via* its strong NOE to the neighbouring Pro[4] H–C(δ) and $H_{(pro\text{-}R)}$ *via* its NOE involving Thr[6] H–C(α). Once more, the predominant conformation in solution is proposed to be a rotamer **I**.

The Pro[4] residue in the macrocyclic system of **2** has an *'endo'* conformation in the crystalline state [5] with respect to the ring puckering, *i.e.* the H–C(γ) and the CO bonds point to the same direction. The angle χ_1 is 36° in the crystalline state, yielding the theoretical coupling constants of 7.3 for $H_{(pro\text{-}S)}$ and 1.2 Hz for $H_{(pro\text{-}R)}$, respectively. The inspection of the E.COSY spectrum yields $^3J(\alpha,\beta) = 8.7$ Hz for the downfield β proton and $^3J(\alpha,\beta) = 4.5$ Hz for the highfield β proton. This is in accordance with the observed NOE between $Me_2Tyr^5CH_3N$ and Pro[4] H'–C(β), leading to the configurational assignment of H'–C(β) as *pro-R*. Therefore, we propose a similiar conformation for both the crystalline and solution state.

The Me_2Tyr^5 residue adopts conformation **I** ($\chi_1 = -41.8°$) in the crystal structure of **2**. We observe homonuclear coupling constants $^3J(\alpha,\beta) = 4.6$ and $^3J(\alpha,\beta') = 11$ Hz, yielding $P_I = 77$, $P_{II} = 19$, and $P_{III} = 4\%$. There is only a very weak correlation to the highfield H′–C(β) in the 'inverse COLOC' spectrum, indicating predominance of rotamer **I**. However, the quantitative information about the size of the heteronuclear coupling constant in an (non-decoupled) 'inverse COLOC' cannot be directly derived as in COLOC itself. This results from different transfer functions which reads for the inverse variant (no refocussing delay Δ_2) to $I \sim \sin\pi\,{}^nJ(C,H)\,\Delta_1\pi\,\cos\pi\,J(H,H)\,\Delta_1$. Hence, the weaker dependence from ${}^nJ(C,H)$ (in COLOC from $\sin\pi\,{}^nJ(C,H)\,\Delta_1\,\sin\pi\,{}^nJ(C,H)\,\Delta_2 \sim \sin^2\pi\,J(C,H)\,\Delta$) renders the interpretation without knowledge of all passive couplings less straightforward.

Thr[6] links the macrocyclic system to the linear side chain, as in various cyclic peptides and depsipeptides [54], *e.g.* stendomycin [55] and telomycin [56]. The structural features of the Thr[6] residue have already been discussed above.

The MeLeu[7] residue is the only D-amino acid present in didemnin A (**1**) and B (**2**). In the crystalline state ($\chi_1 = 60.7°$) as well as in (D_6)DMSO solution, it adopts conformation **I**. The NMR spectroscopic evidence for a similar orientation in solution is as follows. First, $^3J(\alpha,\beta\,(pro\text{-}S)) = 11.1$ Hz and $^3J(\alpha,\beta'\,(pro\text{-}R)) = 5.0$ Hz yield $P_{I,II} = 78$, $P_{II,I} = 22$, and $P_{III} = 0\%$. The predominance of rotamer **I** is confirmed by very weak cross-peaks from CO to both β protons in the 'inverse COLOC' spectrum, and additionally by a strong NOE between MeLeu[7] CH_3–N and MeLeu[7] H–C(β).

In the crystal structure, the Pro[8] ring has the so-called *'exo'* conformation [5] (in contrast to Pro[4]), with C(γ) and the CO group pointing in opposite directions. Additionally, Pro[8] adopts a χ_1 angle of −31° in the crystal structure of **2**, which corresponds to the measured coupling constants. We can extract two coupling constants $^3J(\alpha,\beta) = 7.8$ and $^3J(\alpha,\beta') = 7.4$ Hz. In the COLOC spectrum, weak correlations to both diastereotopic protons are observed.

Comparison of the Conformation of Didemnin A (1) and Didemnin B (2). – Our interest in the conformational analysis of **1** and **2** has been arisen by their differences in the biological acitivites. However, both depsipeptides show very similar NMR data for the macrocyclic part of the molecule indicating very closely related conformations.

A first indication of this homology can be seen from the comparison of chemical-shift values. *E.g.* the differences of the NMR chemical-shift values of *C*=O of residues 1 to 6 are smaller than 0.3 ppm, with the exception of the Hip[2] *C*=O which differs by 0.8 ppm. The temperature gradients (see *Table 4*) of Leu[3] N*H* and Ist[1] N*H* are very small in both **1** and **2** pointing to a related H-bonding pattern. The differences in the experimentally observed H...H distances and the differences in the scalar coupling constants for the residues of the macrocyclic system are within the range of the estimated standard deviations for each of the experiments performed. So, *e.g.* the cross-linking NOE's between Leu[3] N*H* and Thr[6] *H*–C(α) (324 (**2**) and 320 pm (**1**)) and between Ist[1] $H_{(pro\text{-}S)}$–(α) and N*H* (264 (**2**) and 279 pm (**1**)), which are sensitive for the overall conformation of the macrocyclic part, differ only slightly (see *Table 2*).

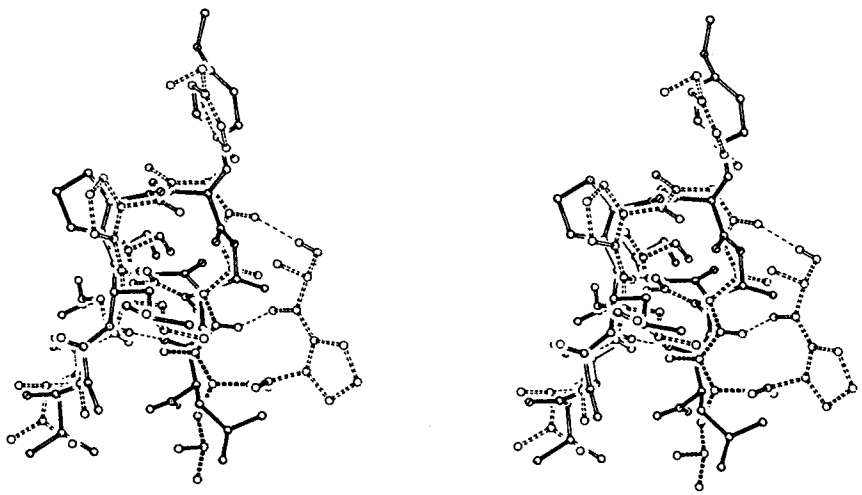

Fig. 10. *Stereoview of a least-squares fit of the averaged conformations of didemnin A* (**1**) *and didemnin B* (**2**) *obtained as a mean over a 70-ps restrained MD trajectory* (*in vacuo*). Only the corresponding backbone atoms of the macrocyclic systems have been fitted to each other yielding a root mean square deviation of 0.51Å for the fitted atoms. The structure of **1** is drawn by open lines, that of **2** by dashed open lines. The part of the MeLeu[7] side chain which shows the main differences is indicated by solid lines for **1** and by dashed solid lines for **2**. Note that the conformations of the side chains are less defined.

In addition, the predominant side-chain conformations, except for MeLeu[7] (see below), are very similar. *E.g.* the corresponding scalar coupling constants $^3J(\alpha,\beta)$ of Me_2Tyr[5] are 4.75 Hz in **1** and 4.5 Hz in **2** for $H_{(pro\text{-}S)}$–C(β) and 10.3 and 11.0 Hz for the $H_{(pro\text{-}R)}$–C(β), respectively. Another example is the Pro[4] residue with $^3J(\alpha,\beta) = 8.7$ Hz for $H_{(pro\text{-}S)}$–C(β) (4.5 Hz for $H_{(pro\text{-}R)}$–C(β)) in **2** as compared to 8.5 Hz (4.0 Hz) for **1**.

Major differences are observed in the orientation of the linear moiety of the didemnins. For **2**, the measured NOE's and coupling constants involving Thr[6] and MeLeu[7] fit well with the geometry observed in the crystal structure. In contrast to these observations,

there is a remarkable discrepancy in $^3J(NH,\alpha)$ of Thr^6, which is 5.7 Hz for **2** *vs.* 10 Hz for **1**, corresponding to a change in the angle ϕ. We should expect $\phi = -75°$ (as well as 25, 95, or $-160°$) for a coupling constant of 5.7 Hz ($-68.6°$ is observed in the crystal structure and is well reproduced by the different calculations) and $-120°$ for a coupling constant of *ca.* 10 Hz. These observations are supported by the corresponding NOE's (r(Thr^6 N*H*,Thr^6) *H*–C(α) = 276 pm (289 pm in the crystal structure) for **2** and 310 pm for **1**). In addition, a NOE between the MeLeu^7 C*H*$_3$N and the Ist$^1\alpha_{(pro\text{-}S)}$ protons (330 pm) is detected for **1** which confirms the different orientation of the CH$_3$N vector, pointing towards Ist^1 in **1** (see *Fig. 10*) and in the opposite direction in **2** (in the crystal and solution structure). The latter orientation is confirmed by a NOE for **2** between MeLeu^7 C*H*$_3$N and Thr^6 N*H* (260 pm) which cannot appear in the other conformation.

On Using 'NMR Structures' as *Patterson* Search Models to Resolve the Crystal Structure of Didemnin B(2). – The very powerful statistical direct methods [57] [58] of crystal-structure solution are not quite omnipotent and usually fail for organic structures with more than *ca.* 200 independent C-, N- and O-atoms per asymmetric unit, or when the experimental data do not extend to 'atomic resolution' (*ca.* 1 Å). However, no sharp dividing line can be drawn because of the influence of space group, data quality, luck, and last but not least computer time.

The alternative '*Patterson search*' approach [59] [60] does not require atomic resolution and is less critically limited by the size of the structure. However, it requires additional chemical information in the form of a search fragment. We investigate here the suitability of structures obtain from NMR data for this approach. We have tested two different structural fragments each of which corresponds to an energy minimum and fulfills the observed distance restraints quite well. The first fragment used (see *Table 9*) contains 60 atoms of **2** (mainly in the macrocyclic system), calculated with MOMO using the distance restraints. The search fragment yields a fractional scattering power of 73%.

Table 9. *Data on the Solution of the Known Crystal Structure of Didemnin B* (**2**) ($C_{57}H_{89}N_7O_{15} \cdot 1.5\ C_6H_6 \cdot H_2O$) *with the* Patterson *Search Program PATSEE*[a])

Space group	$C222_1$	$C222_1$
Model size (atoms)	41	60
Scattering power	0.52	0.73
Model obtained with	GROMOS[b])	MOMO[c])
Number of rotational trials	50000	50000
RFOM^f/RFOM^c	1.03[2][d])	1.01[3]
$E_{calc/obs}{}^f/E_{calc/obs}{}^c$	0.98[2][d])	0.92
Number of translational trials	15000[d])	10000
TPRSUM^f/TPRSUM^c	0.81[1][d])	1.15[2]
$R_E(1)/_E(2)^c/R_E(1)/_E(2)^f$	1.09/1.09[1][d])	0.95/1.00[2]
CFOM^f/CFOM^c	0.98[1][d])	1.02[2]

[a]) The calculations were performed on an *IBM3090*-mainframe computer. For the description of the procedure and the definition of the various figures of merit [60].

[b]) The lowest-energy conformation was picked from the trajectory of the 70-ps restrained MD simulation.

[c]) Energy-minimized conformation of the MOMO calculation including distance restraints.

[d]) Obtained after a subsequent (10000 rotational trials) rotational refinement. The superscript ^{c} refers to the correct, ^{f} to the highest-ranked wrong solution. In each case, the rank of the solution is given in brackets (1 = best solution, 2 = second-best solution, *etc.*).

After performing 50000 rotational trials, the third-ranked (according to the RFOM figure of merit [61a]) solution yields the highest $E_{calc/obs}$ value. The subsequent translation search (10000 trials) for this orientation yields the correct solution (showing almost all of the non-H-atoms after applying a tangent expansion and *Fourier* recycling procedure) ranked as second best. A least-squares fit of the search fragment with the backbone atoms of the macrocyclic ring of the crystal structure leads to a r.m.s. deviation of 0.28 Å.

The second fragment used consists of 41 atoms of the lowest-energy conformation of **2**, picked up from the trajectory of the 70-ps restrained GROMOS calculation. The fragment yields a fractional scattering power of 52%. Once more, we have performed a least-squares fit to the 23-membered ring of the crystal structure, leading to a r.m.s. deviation of 0.40 Å. The 50000 rotational trials during the orientation search reveal a number of different orientations judged according to the RFOM figure of merit. The fourth-ranked orientation shows the best $E_{calc/obs}$ value and is submitted to an orientational refinement run. The second-best orientation of this refinement procedure leads to the correct solution (ranked second), after a subsequent translation search (10000 trials). This solution is again tested by a tangent expansion and *Fourier* recycling calculation (a SHELXS-86 feature [61]) which leads to the correct crystal structure.

In principle, there is no doubt about the power of the *Patterson* search approach to solve crystal structures [62] or the ability of modern NMR spectroscopy to generate high-quality solution structures [17]. Nevertheless, there are some pitfalls in practice. Firstly, the structure derived from NMR data and modelling is an averaged structure. So, if the molecules of interest possess large rigid domains, the NMR information will be sufficient to model a well defined structure which could serve as a search fragment to solve the crystal structure. In the case of molecules with a large amount of flexibility, the fraction of atomic positions which will subsequently fit well to the corresponding atomic positions in the crystal structure might be too low. We would propose as a crude guideline that the search model must yield a fractional scattering power of more than 30% if there are overall positional r.m.s. deviations of *ca.* 0.1 to 0.3 Å. Even with a fragment of scattering power of more than 50% and showing an r.m.s. deviation from the atomic positions in the crystal structure of 0.40 Å, it has been difficult to obtain the correct solution ranked first according to the various figures of merit. However, again no sharp dividing line can be drawn, and success will depend on a number of factors. In addition, we should point out that there is no necessity that the conformation in solution and in the crystalline state are identical [63]. In particular, H-bonds tend to prefer intramolecular orientations in solution, whereas in crystal structures, they are often intermolecular [15] [35] [63].

Concluding Remarks. – We have applied two modelling techniques which follow different philosophies: the well established GROMOS program package as a MD approach and MOMO, a PC-oriented modeling system representing the MM approach.

In our experience, MOMO is suited to model a solution using distance restraints, but with some reservations. It is inherent to the MM method that there is no way to jump between two conformations both of which represent energy minima. However, the incorporation of NOE data in form of a pseudo potential makes it possible to escape from a local minimum. We are aware that this approach can only serve as a crude model builder. We do not employ the average character of the NOE distances in a physically

correct manner, but use them as fixed distances smoothed by the allowance of a deviation from the target value. The way of considering the NOE restraints in the MD simulations as mean distances with respect to time is physically more appropriate.

If we start the modelling with an adequate initial structure (in our case the crystal structure), it seems possible to obtain a reasonable result consistent with the NMR data. In our experience, current 'distance geometry' programs often fail to propose a reasonable start structure automatically, so the chemist is forced to intervene and select structures intuitively.

A problem which affects both of the employed programs is the quality of the force field. So, *e.g.* the planarity of the amide or ester moiety is not adequately maintained. This can be traced back to an unsuitable weighting of the force constants used for the NOE restraints relative to those describing, *e.g.*, the torsional potential. A relative large force constant for the restraint potential has to be used to find a global rather than a local minimum, which may lead to significant deformation of 'standard geometries'.

However, we conclude that in most cases, especially for smaller molecules starting with adequate initial geometry, the combined 'distance geometry' and MM approach incorporated in MOMO provide an efficient path to a realistic image of the 'solution structure'.

Finally, the conformational analysis of the didemnins has been performed in order to understand the marked difference of the biological activity of didemnin A (**1**) and (**2**). We suggest that these differences can hardly be ascribed to conformational effects, but rather to the different constitutions, because both molecules exhibit very similar backbone and side-chain conformations in DMSO solution. The detected conformational change concerning the MeLeu[7] residue seems insufficient to explain the disparity in biological activity.

We gratefully acknowledge financial support by the *Deutsche Forschungsgemeinschaft*, the *Fonds der Chemischen Industrie*, and the *Bundesministerium für Forschung und Technologie*. Samples were kindly provided by Dr. *van der Helm*, University of Oklahoma, Dr. *A.J. Weinheimer*, University of Houston, and Prof. Dr. *U. Schmidt*, Universität Stuttgart. We thank Dr. *W. Bermel, Bruker GmbH*, Karlsruhe, for obtaining the 'inverse COLOC' spectrum with selective excitation. We thank Dr. *W. van Gunsteren*, University of Groningen, for providing us with the GROMOS program system.

Measurement Conditions. – *General.* All spectra were recorded on an *AM 500* spectrometer ($\nu_o(^1H)$ 500 MHz) with an *Aspect-3000* computer (*Bruker*). The measurements were performed at 300 K, using the standard software if not otherwise stated. Concentrations: ^{1}H-NMR and ^{13}C-NMR spectra, 20 mg/0.5 ml in degassed $(CD_3)_2SO$

2. *$^1H,^1H$-DQF-COSY Spectrum.* Sequence: Δ_0-90°$_x$-t_1-90°$_y$-Δ_1-90°$_x$-t_2. Relaxation delay 1.5 s, $\Delta_1 = 3$ µs, sweep width 5102 Hz, 1 K experiments with size 4 K in f_2, quad detection, single zero filling in t_1 and apodization with a squared shifted sine bell (SSB factor 3) in both dimensions.

3. *$^1H,^1H$-TOCSY Spectrum.* Sequence: Δ_0-90°$_\phi$-t_1-MLEV17-t_2. Relaxation delay 1.5 s, mixing time 50 ms, sweep width 5102 Hz, 1 K experiments with size 4 K in f_2, quad detection, single zero filling in t_1, baseline correction, and apodization with a squared shifted sine bell (SSB factor 3) in both dimensions.

4. *$^1H,^1H$-E.COSY Spectrum at 300 K.* Pulse sequence D_0-$\pi/2\beta$-t_1-$\pi/2\beta$-$\pi/2$-aq. 1200 experiments, ($\beta_0 = 20$ scans, $\beta_1 = \beta_7 = 16$ scans, $\beta_2 = \beta_4 = \beta_6 = 4$ scans, $\beta_3 = \beta_5 = 2$ scans), weigthing factors ($DC_0 = DC_2 = DC_4 = DC_6 = 1$, $DC_1 = DC7 = -1.067$, $DC_3 = DC_5 = -1.176$), relaxation delay 1.5 s, size 4 K in $F2$, spectral width in $F2$ and $F1$ 3200 Hz, zero filling to 8 K in $F2$ and 2 K in $F1$, *Lorentz* to *Gauss* multiplication in both dimensions ($GB = 0.15$, $LB = -1.5$).

5. *$^1H,^1H$-NOESY Spectrum* (pure absorption *via* TPPI [64]). Sequence: Δ_0-90°$_x$-t_1-90°$_x$-τ_m-90°$_x$-t_2. Relaxation delay 1.5 s, spectra with different mixing times $\tau_m = 50$ msec, $\tau_m = 100$ msec, $\tau_m = 150$ msec, and $\tau_m = 200$ msec

were recorded, sweep width 5102 Hz, 1 K experiments with size 4 K in f_2, quad detection, single zero filling in t_1, baseline correction, and apodization with a squared shifted sine bell (SSB factor 3) in both dimensions. For the processing and the determination of the build-up rates, the '2DNMR' program of *Kaptein* and *Boelens* [30] was applied.

6. *^1H,^{13}C-'Inverse-COLOC' spectrum.* Sequence: A_0-90°(^{1}H)-A_1-90°$_{selective}$(^{13}C)-t_1/2-180°(^{1}H)-t_1/2-90°(^{13}C)-t_2(^{1}H). Relaxation delay 1.5 s, A_1 = 50 ms, sweep width in f_1 5102 Hz and f_2 5208 Hz, 660 experiments with size 4 K in f_2, zero filling in t_1 to 2 K, and apodization with a squared shifted sine bell (SSB factor 3) in both dimensions, t_1, ridges were eliminated by subtracting an appropriate row of the 2D spectra from the 2D matrix. The absolute-value spectrum was recorded and processed in the power mode.

REFERENCES

[1] K.L. Rinehart, Jr., J.B. Gloer, J.C. Cook, Jr., S.A. Mizsak, T.A. Scahill, *J. Am. Chem. Soc.* **1981**, *103*, 1857.

[2] K.L. Rinehart, Jr., J.B. Gloer, R.G. Hughes, Jr., H.E. Renis, J.P. McGovren, E.B. Swynenberg, D.A. Stringfellow, S.L. Kuentzel, L.H. Li, *Science* **1981**, *212*, 933.

[3] K.L. Rinehart, V. Kishore, S. Nagarajan, R.J. Lake, J.B. Gloer, F.A. Bozich, K.-M. Li, R.E. Maleczka, Jr., W.L. Todsen, M.H.G. Munro, D.W. Sullins, R. Sakai, *J. Am. Chem. Soc.* **1987** *109*, 6846.

[4] U. Schmidt, M. Kroner, H. Griesser, *Tetrahedron Lett.* **1988**, *29*, 3057.

[5] M.B. Hossain, D. van der Helm, J. Antel, G.M. Sheldrick, S.K. Sanduja, A.J. Weinheimer, *Proc. Natl. Acad. Sci. U.S.A.* **1988**, *85*, 4118.

[6] H. Kessler, G.M. Sheldrick, J. Antel, M. Will, *Magn. Reson. Chem.* **1988**, *26*, 501.

[7] K.L. Rinehart, V. Kishore, K.C. Bible, R. Sakai, D.W. Sullins, K.-W. Li, *J. Nat. Prod.* **1988**, 10.

[8] S.L. Crampton, E.G. Adams, S.L. Kuentzel, L.H. Li, G. Badiner, B.K. Bhuyan, *Cancer Res.* **1984**, *44*, 1796.

[9] K.L. Rinehart, Jr., J.B. Gloer, G.R. Wilson, R.G. Hughes, Jr., L.H. Li, H.E. Renis, J.P. McGovren, *Fed. Proc.* **1983**, *42*, 90.

[10] T.L. Jiang, R.H. Lin, S.E. Salman, *Cancer Chemother. Pharmacol.* **1983**, *11*, 1.

[11] H.G. Chun, B. Davies, D. Hogh, M. Suffness, J. Plowman, K. Flora, C. Grieshaber, B. Leyland-Jones, *Invest. New Drugs* **1986**, *4*, 279.

[12] L.H. Li, L.G. Timmins, T.L. Wallace, W.C. Krueger, M.D. Prairie, W.B. Im, *Cancer Lett.* **1984**, *23*, 279.

[13] D.W. Montogomery, C.F. Zukosky, *Transplantation* **1985**, *40*, 49.

[14] D.W. Montogomery, R. Kibler, B. Poulos, C.F. Zukosky, D.H. Russell, *Fed. Proc.* **1987**, *44*, 634.

[15] H.-R. Loosli, H. Kessler, H. Oschkinat, H.-P. Weber, T.J. Petcher, A. Widmer, *Helv. Chim. Acta* **1985**, *68*, 682.

[16] H. Kessler, M. Gehrke, C. Griesinger, *Angew. Chem. Int. Ed.* **1988**, *27*, 490, and ref. cit. therein.

[17] H. Kessler, H. Oschkinat, H.R. Loosli, in 'Two-Dimensional NMR Spectroscopy', Eds. W.R. Croasmun and R.M.K. Carlson, Verlag Chemie, Weinheim, 1987, pp. 259–299.

[18] H. Kessler, W. Bermel, A. Müller, K.H. Pook, 'The Peptides: Analysis, Synthesis, Biology', Eds. S. Udenfriend, J. Meienhofer, and V. Hruby, Verlag Chemie, Weinheim, 1986, Vol. 7, pp. 437–472.

[19] a) L. Braunschweiler, R.R. Ernst, *J. Magn. Reson.* **1983**, *53*, 521; b) A. Bax, R.A. Byrd, A. Azalos, *J. Am. Chem. Soc.* **1985**, *106*, 7632.

[20] a) W. Bermel, C. Griesinger, K. Wagner, *J. Magn. Reson.* **1988**, in press; b) H. Kessler, G.M. Sheldrick, J. Antel, M. Will, *Magn. Reson. Chem.* **1988**, *26*, 501.

[21] a) W.P. Aue, E. Bartholdi, R.R. Ernst, *J. Chem. Phys.* **1976**, *64*, 2229; b) M. Rance, O.W. Sørensen, G. Bodenhausen, G. Wagner, R.R. Ernst, K. Wüthrich, *Biochem. Biophys. Res. Commun.* **1983**, *117*, 479.

[22] a) J. Jeener, B.H. Meier, P. Bachmann, R.R. Ernst, *J. Chem. Phys.* **1979**, *71*, 4546; b) J.H. Noggle, R.E. Schirmer, 'The Nuclear Overhauser Effect', Academic Press, New York, 1971.

[23] a) K. Wüthrich, 'NMR of Proteins and Nucleic Acids', Wiley, New York, 1986; b) V.F. Bystrov, *Progr. NMR Spectrosc.* **1976**, *10*, 41.

[24] H. Kessler, H.R. Loosli, H. Oschkinat, *Helv. Chim. Acta* **1985**, *68*, 661.

[25] L. Müller, *J. Am. Chem. Soc.* **1979**, *101*, 4481.

[26] a) H. Oschkinat, R. Freeman, *J. Magn. Reson.* **1984**, *60*, 164; b) H. Kessler, H. Oschkinat, C. Griesinger, *Magn. Reson. Chem.* **1986**, *70*, 106.

[27] H. Kessler, H. Oschkinat, *Angew. Chem.* **1985**, *97*, 689.

[28] H. Kessler, A. Müller, H. Oschkinat, *Magn. Reson. Chem.* **1985**, *23*, 844.

[29] a) C. Griesinger, O.W. Sørensen, R.R. Ernst, *J. Am. Chem. Soc.* **1985**, *107*, 6394; b) *J. Chem. Phys.* **1986**, *85*, 6837; c) *J. Magn. Reson.* **1987**, *75*, 474–492.

[30] R. Kaptein, R. Boelens, 2DNMR/VMS Version 8602, Laboratory of Organic Chemistry, University of Utrecht, The Netherlands, 1988.
[31] H. Beck, E. Egert, to be published.
[32] J. Åquist, W.F. van Gunsteren, M. Leijonmark, O.J. Tupia, *J. Mol. Biol.* **1985**, *183*, 461.
[33] W.F. van Gunsteren, R. Kaptein, E.R.P. Zuiderweg, Proceedings of the NATO/CECAM Workshop on Nucleic-Acid Conformation and Dynamics, Ed. W.K. Olsen, Orsay, 1983, pp.79–92.
[34] W.F. van Gunsteren, R. Boelens, R. Kaptein, R.M. Scheek, E.R.P. Zuiderweg, 'Molecular Dynamics and Protein Structure', Ed. J. Hermans, Polycrystal Book Service, Western Springs, 1985, pp.92–99.
[35] H. Kessler, J.W. Bats, C. Griesinger, S. Koll, M. Will, K. Wagner, *J. Am. Chem. Soc.* **1988**, *110*, 1022.
[36] a) J. Lautz, H. Kessler, R. Kaptein, W.F. van Gunsteren, *J. Computer-Aided Mol. Design* **1987**, *1*, 219; b) J. Lautz, Dissertation, Universität Frankfurt, 1988.
[37] H.J. Lindner, *Tetrahedron* **1974**, *30*, 1127.
[38] H.J. Lindner, private communications (Technische Universität, D–6100 Darmstadt).
[39] J. Gasteiger, M. Marsilli, *Tetrahedron* **1980**, *36*, 3219.
[40] H.J.C. Berendsen, J.P.M. Postma, W.F. van Gunsteren, A. DiNola, J.R. Haak, *J. Chem. Phys.* **1984**, *81*, 3684.
[41] a) R. Fletcher, C.M. Reeves, *Comput. J.* **1964**, *7*, 149; b) W.F. van Gunsteren, M. Karplus, *J. Comput. Chem.* **1980**, *7*, 266.
[42] H. Kessler, *Angew. Chem. Int. Ed.* **1982**, *21*, 512.
[43] H. Kessler, H. Oschkinat, H.R. Loosli, in 'Methods in Stereochemical Analysis', Eds. A. Takeuchi and P. Marchand, Verlag Chemie, Deerfield Beach, FL, 1987, Vol. 9, pp. 259–299.
[44] R. Rowan, A. Warshel, B.D. Sykes, M. Karplus, *Biochemistry* **1974**, *13*, 970.
[45] J.A. Smith, L.G. Pease, *CRC Crit. Rev. Biochem.* **1980**, *19*, 315.
[46] L.M. Gierasch, C.M. Deber, V. Madison, C.H. Niu, E.R. Blout, *Biochemistry* **1981**, *20*, 4730.
[47] I.L. Karle, in 'The Peptides: Analysis, Synthesis, Biology', Eds. S. Udenfriend, J. Meienhofer, and V. Hruby, Academic Press, New York, 1981, Vol.4, pp. 1–54.
[48] J.P. Snyder, *J. Am. Chem. Soc.* **1984**, *106*, 2393.
[49] IUPAC-IUB Commission, *Eur. J. Biochem.* **1984**, *138*, 9.
[50] H. Kessler, C. Griesinger, K. Wagner, *J. Am. Chem. Soc.* **1987**, *109*, 6927.
[51] K.G.R. Pachler, *Spectrochim. Acta* **1963**, *19*, 2085.
[52] K.G.R. Pachler, *Spectrochim. Acta* **1964**, *20*, 581.
[53] V.F. Bystrov, *Prog. Nucl. Magn. Reson. Spectrosc.* **1976**, *10*, 41.
[54] Y.A. Ovchinnikov, V.T. Ivanov, *Tetrahedron* **1975**, *31*, 2177.
[55] T.P. Pitner, D.W. Urry, *Biochemistry* **1972**, *11*, 4132.
[56] a) N.G. Kumar, D.W. Urry, *Biochemistry* **1973**, *12*, 3811; b) *ibid.* **1973**, *12*, 4392.
[57] J. Karle, *Angew. Chem.* **1986**, *98*, 611.
[58] H. Hauptmann, *Angew. Chem.* **1986**, *98*, 600.
[59] C.E. Nordman, *Acta Crystallogr., Sect. A* **1972**, *28*, 134.
[60] E. Egert, G.M. Sheldrick, *Acta Crystallogr., Sect. A* **1985**, *41* 262.
[61] G.M. Sheldrick, 'SHELXS-86', in 'Crystallographic Computing 3', Eds. G.M. Sheldrick, C. Krüger, and R. Goddard, Oxford Univ. Press, Oxford, 1985, pp. 175–189.
[62] V.J. van Geerestein, J.A. Kanters, H. van Koningsveld, *Acta Crystallogr., Sect. B* **1987**, *43*, 92.
[63] H. Kessler, G. Zimmermann, H. Förster, J. Engel, G. Oepen, W.S. Sheldrick, *Angew. Chem. Int. Ed.* **1981**, *20*, 1053.
[64] D. Marion, K. Wüthrich, *Biochem. Biophys. Res. Commun.* **1983**, *113*, 967.